Phytoplanktonic response to simulated volcanic and desert dust deposition events in the South Indian and Southern Oceans

Carla Geisen, Céline Ridame, Emilie Journet, Pierre Delmelle, Dominique Marie, Claire Lo Monaco, Nicolas Metzl, Rawaa Ammar, Joelle Kombo, Damien Cardinal

LIMNOLOGY and OCEANOGRAPHY

ASLO

Limnol. Oceanogr. 67, 2022, 1537–1553

doi: 10.1002/lno.12100

Phytoplanktonic response to simulated volcanic and desert dust deposition events in the South Indian and Southern Oceans

Carla Geisen,[1*] **Céline Ridame**,[1*] **Emilie Journet**,[2] **Pierre Delmelle**,[3] **Dominique Marie**,[4] **Claire Lo Monaco**,[1] **Nicolas Metzl**,[1] **Rawaa Ammar**,[2,3] **Joelle Kombo**,[1] **Damien Cardinal**[1]

[1]Sorbonne Université, LOCEAN—IPSL Laboratoire d'Océanographie et du Climat, Expérimentations et Approches Numériques, UMR 7159, (SU CNRS MNHN IRD), Paris, France
[2]LISA (Laboratoire Interuniversitaire des Systèmes Atmosphériques), UMR 7583, CNRS, Université Paris-Est Créteil et Université de Paris, Institut Pierre Simon Laplace (IPSL), Créteil, France
[3]Earth and Life Institute, Environmental Sciences, UCLouvain, Louvain-la-Neuve, Belgium
[4]CNRS, Sorbonne Université, UMR 7144 Adaptation et Diversité en Milieu Marin, Roscoff, France

Abstract

Contrasting concentrations of macronutrients and micronutrients induce different nutrient limitations of the oceanic productivity and shape the composition of the phytoplankton communities of the South Indian Ocean and Indian sector of the Southern Ocean. o assess the phytoplankton response to nutrient release by desert dust and volcanic ash aerosols in these distinct biogeochemical regions, we conducted microcosm incubation experiments. A dry or wet deposition of either dust from Patagonia or ash from the Icelandic volcano Eyjafjallajökull or dissolved nutrients (Si, Fe, N and/or P) were added to trace metal clean incubations of surface seawater collected from five stations. These deposition experiments enabled the measurement of the biological response along with solubility calculations of nutrients. Both types of aerosols alleviated the iron deficiency occurring in the Southern Ocean during austral summer and resulted in a 24–110% enhancement of the primary production, depending on the station. The release of dissolved silicon may also have contributed to this response, although to a lesser extent, whereas neither the dust nor the ash relieved the nitrogen limitation in the low-nutrient and low-chlorophyll area. Diatom growth was responsible for 40% to 100% of the algal biomass increase within the responding stations, depending on the region and aerosol type. The high particle concentrations that are characteristic of ash deposition following volcanic eruptions may be of equal or higher importance to phytoplankton compared to desert dust, despite ashes' lower nutrient solubility to the ocean.

The Southern Ocean is the largest high-nutrients low-chlorophyll (HNLC) area of the ocean, where phytoplankton growth is mostly limited by low surface iron (Fe) concentrations (Martin 1990; Moore et al. 2002). Due to latitudinal gradients of dissolved macronutrients decreasing northwards, the Southern Ocean can be further divided in distinct biogeochemical regions (Fig. 1), characterized by different nutrient limitations. In the Subantarctic Zone, dissolved inorganic phosphorus (DIP) and NO_x ($NO_3^- + NO_2^-$) remain high but dissolved silicon (Si) is scarce (Nelson et al. 2001). The Fe limitation of the Antarctic Zone is thus shifted to a Fe-Si co-limitation (Hutchins et al. 2001; Hoffmann et al. 2008), referred to as high nitrate-low silicon-low chlorophyll (HN-LSi-LC) (Dugdale et al. 1995). Further north, the Subtropical Front marks the boundary with the low-nutrient low-chlorophyll (LNLC) region of the Subtropical Zone of the South Indian Ocean. This region within the oligotrophic subtropical gyre is characterized by low NO_x and surface chlorophyll *a* (Chl *a*) concentrations (McClain et al. 2004; Morel et al. 2010).

One of the factors responsible for the Fe-depletion in the surface Southern Ocean is the shortage of the so-called new Fe supply, that is, the input of Fe from outside the euphotic

*Correspondence: carla.geisen@univ-littoral.fr, celine.ridame@locean.ipsl.fr

Additional Supporting Information may be found in the online version of this article.

Author Contribution Statement: C.G., C.R. and D.C. designed the experiments and analyzed the data. C.G. and C.R. performed the onboard experiments. C.G., J.K. and D.M. performed the laboratory analyses and C.R. the statistical analyses. E.J. and P.D. provided the natural aerosols and R.A. performed their characterization. C.L.M. was chief scientist of the OISO-29 oceanographic campaign. C.G., C.R. and D.C. wrote the manuscript and all the authors contributed significantly in writing and editing the manuscript and its revisions.

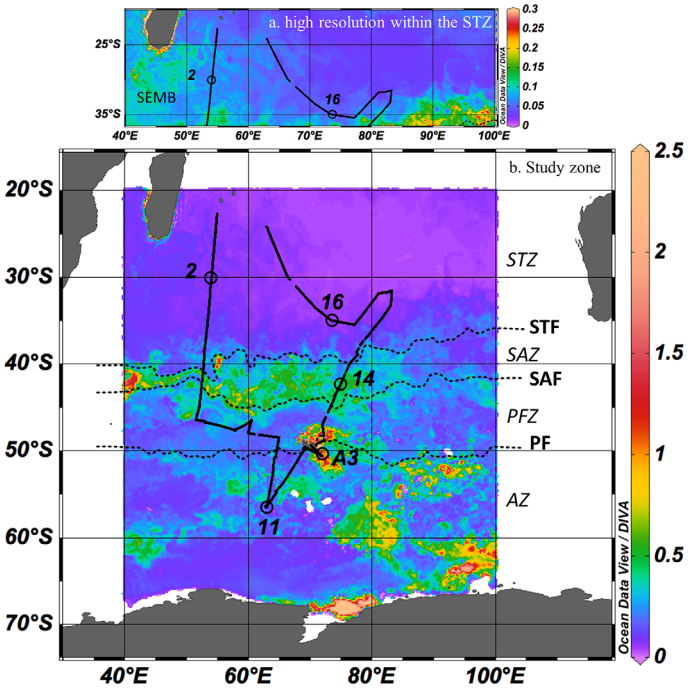

Fig. 1. OISO-29 cruise transect showing the locations of the five stations (LNLC-2, HNLC-11, Kerguelen-A3, HN-LSi-LC-14 and LNLC-16) where the bioassay experiments were performed, and satellite-derived Chl *a* concentration (μg L^{-1}) averaged over January 2019 (MODIS). The position of major fronts was determined from satellite-derived temperature data (January 2019, MODIS): STF, Subtropical Front (18°C); SAF, Subantarctic Front (13°C); PF, Polar Front (5°C). Fronts delimit: STZ, Subtropical Zone; SAZ, Subantarctic Zone, PFZ: Polar front zone; AZ, Antarctic Zone. The map (**a**) shows the STZ with a higher chlorophyll *a* concentration scale adjustment than the general map (**b**), thus enabling the detection of the south East Madagascar Bloom (SEMB). Maps were produced using Ocean Data View (Schlitzer 2021).

zone. In winter, surface Fe is mainly supplied by vertical deep mixing (Tagliabue et al. 2014). As the fluvial Fe supply to the remote Southern Ocean can be neglected, aerosol deposition may be episodically a significant external source of Fe for the open surface waters during the summer stratified period, except in upwelling areas associated to hydrothermal vents, or in areas subjected to Fe-rich sea ice melting, or within naturally fertilized coastal regions such as the Kerguelen and Crozet plateaus (Ardyna et al. 2019). The monthly averaged dust deposition flux to the Southern Ocean is very low (10–45 mg m^{-2} month^{-1} during austral summer, Meskhidze et al. 2007), but intense sporadic events may affect phytoplankton growth. These events occur especially during the austral summer months, when the water column is stratified and the emissions from the Patagonian source are more frequent (Gassó and Torres 2019). Several studies suggest that the dust deposition to the Southern Ocean was up to 20 times higher during the Last Glacial Maximum (Mahowald et al. 1999). At this time, dust-mitigated Fe input to the ocean surface layer may have fertilized the ocean phytoplankton production, thereby contributing to millennial-scale CO_2 fluctuations associated with glacial–interglacial cycles (Martin 1990; Watson et al. 2000; Conway et al. 2015).

Several studies have also shown that volcanic ash is a significant source of dissolved Fe that can stimulate phytoplankton growth in HNLC regions (Olgun et al. 2011; Mélançon et al. 2014). Clear evidence has been provided by direct observation after the 2008 eruption of the Kasatochi volcano in the Gulf of Alaska (Langmann et al. 2010). The range of ash deposition to the ocean is highly variable (Durant et al. 2010) and is influenced by various factors, such as the volume of ejected ash, the ash grain distribution and in-plume processes (Duggen et al. 2010; Ayris and Delmelle 2012).

Several mesoscale artificial Fe enrichment experiments (Boyd et al. 2007 and references therein) have demonstrated the relief of the Fe limitation for phytoplankton growth in the Southern Ocean, and microcosm studies have highlighted a biological response after dust or ash additions to its Atlantic sector (Browning et al. 2014; Trimborn et al. 2017). Nevertheless, the Indian and Southern Oceans represent a large ocean basin in which the biological and biogeochemical responses to atmospheric deposition events are poorly documented. To better assess the impact of desert dust and volcanic ash deposition events to this under-sampled region, we performed short term (2 days) microcosm experiments with representative aerosol particle concentrations. Phytoplankton primary production (PP) and community composition were measured after simulated dry or wet aerosol deposition or dissolved nutrients additions. The novelties of this study are the comparison of the nutrient release and phytoplanktonic responses between (i) dust and ash deposition events, (ii) HNLC and LNLC areas, and (iii) dry and wet deposition modes.

Materials and methods

Cruise transect, hydrological, and biogeochemical context

Our study was part of the VT163/OISO-29 (MD217) cruise (Lo Monaco and Metzl 2019), on board the R/V *Marion Dufresne* during the austral summer, from 05 January to 15 February 2019. Experiments were performed at five stations, located in the contrasted LNLC, HN-LSi-LC, and HNLC areas defined by major fronts (Fig. 1), as well as a reference station of the bloom area of the naturally Fe-fertilized Kerguelen plateau (Sta. A3) (Blain et al. 2007; Fripiat et al. 2011).

Bioassay experiments

We carried out trace metal clean nutrient/aerosol additions during bioassay experiments at five stations (Fig. 1, and details in Table 1). All materials were acid-washed (HCl Suprapur) and manipulations took place under laminar flow hoods. Unfiltered surface seawater (~ 10 m depth) was collected within the surface mixed layer using Go-Flo bottles and Kevlar wire to avoid trace metal contamination. Dry deposition events of desert dust or volcanic ash were simulated by adding

Table 1. Experimental nutrient and aerosol additions performed in triplicate at each station, with mono-nutrient and multiple nutrient additions: +Fe (2 nmol L^{-1} $FeCl_3$); +Si (2 μmol L^{-1} Na_2SiO_3); +FeSi (2 nmol L^{-1} $FeCl_3$ + 2 μmol L^{-1} Na_2SiO_3); +N (2 μmol L^{-1} $NaNO_3$); +NP (2 nmol L^{-1} $NaNO_3$ + 0.2 μmol L^{-1} KH_2PO_4), and single aerosol additions of +Dust (2 mg L^{-1}) and +Ash (25 mg.L^{-1}). At Sta. 11, simulated dry and wet deposition events were performed. The control corresponds to unamended seawater.

Region	Station	Zone	Control	+Dust	+Ash	+Fe	+Si	+FeSi	+N	+NP
LNLC	2	STZ	+	Dry	Dry	+	+	+	+	+
LNLC	16	STZ	+	Dry	Dry	+	+	+	+	+
HN-LSi-LC	14	SAZ	+	Dry	Dry	+	+	+		
Plateau	A3	AZ	+	Dry	Dry	+	+	+		
HNLC	11	AZ	+	Dry/wet	Dry/wet	+				

STZ, Subtropical Zone; SAZ, Subantarctic Zone; AZ, Antarctic Zone.

aerosols at final particle concentrations of 2 and 25 mg L^{-1} for the dust and ash treatments, respectively (see below for details about the aerosols). All treatments were performed in triplicate in 2.3-L polycarbonate bottles. Possible trace metal contamination of the surface seawater from the added nutrient solutions was tested (Supporting Information Text S1).

Additional wet deposition events of dust and ash were simulated at HNLC-11 (Table 1). Artificial rainwater was prepared following the protocol described by Paris et al. (2011). Briefly, 100 mg L^{-1} dust or 1250 mg L^{-1} ash ($n = 1$) were added to ultrapure water (Millipore®, resistivity of 18.2 MΩ cm^{-1}) previously acidified with sulfuric acid (1‰ H_2SO_4 SupraPur® at 2×10^{-2} mol L^{-1}, theoretical pH of 4.7). After a contact time of 60 min, 2% of the unfiltered artificial rainwater was added to the incubation bottles filled with unfiltered surface seawater, thus obtaining the same particle concentrations as in the dry deposition mode. Subsamples were filtered through a 0.2-μm polycarbonate membrane for the detection of dissolved macronutrients and Fe concentrations in artificial rainwater.

Before aerosol/nutrient additions, one seawater sample was taken for the determination of the initial PP, pigments and cellular abundances, and replicate samples ($n = 3$) were collected for dissolved macronutrient and Fe concentrations. After aerosol/nutrient additions, the microcosms were incubated for 48 h in on-deck incubators with circulating surface seawater equipped with blue filters (Lee Filters) to simulate the appropriate temperature and irradiance encountered at 10 m depth. The PP was determined between 24 and 48 h for all treatments, whereas the samples used for other analyses were collected at the end of the experiment (48 h).

Abiotic dissolution experiments

To monitor the abiotic release of nutrients at all stations, 250 mL of 0.2-μm filtered surface seawater was introduced into triplicate polycarbonate bottles and amended with the same aerosol concentration and under the same deposition mode as in the bioassay experiments. An additional, abiotic wet deposition performed at HNLC-11 consisted in adding 2% of unfiltered artificial rainwater into 0.2-μm filtered seawater. Bottles were then placed in the same experimental conditions as microcosms. Subsamples were collected after 48 h for the dissolved macronutrients and Fe concentrations. For back-calculations of Fe release in the ash amended artificial rainwater, we used supplementary subsamples filtered after 12 h (refer to Eq. 1).

Characterization of dust and ash

Aerosol collection and deposition

Collection took place in remote areas using clean sampling techniques and samples were stored in double zip bags to avoid anthropogenic contamination.

Desert dust

The fine fraction (< 20 μm) of a Patagonian arid surface soil (south of Sierra Grande, Argentina, hereafter referred to as Pata) was used in all experiments. Dust from this region has been shown to reach the Southern Ocean (Li et al. 2008; Gili et al. 2016). This material corresponds to the first top centimeters of the surface soil exposed to wind erosion. The soil was dry sieved in order to produce a dust analogue (Guieu et al. 2010), hereafter referred to as aerosol for simplification, according to the protocol described by Guieu et al. (2014). The dust concentration used in this study (2 mg L^{-1}) corresponds to an estimated deposition event of 9 g m^{-2} diluted in the upper first meters (*see* details in Supporting Information Text S2). Local dust deposition rates in the Southern Ocean are low (annual mean deposition of 8.0 mg m^{-2} d^{-1}; Li et al. 2008). Thus, this deposition rate is probably overestimated for present-day conditions in the Indian and Southern Oceans, but is assumed to be realistic for the Last Glacial Maximum (Mahowald et al. 1999; Conway et al. 2015) and for other offshore oceanic areas such as the modern open Mediterranean Sea (Ternon et al. 2010). The chosen particle concentration is also in agreement with those used in several microcosm studies performed in LNLC and HNLC areas (Mills et al. 2004; Marañón et al. 2010; Mélançon et al. 2016).

Volcanic ash

The ash originated from the 2010 explosive eruption of the Eyjafjallajökull volcano (63°37′11″N, 19°36′54″W) in Iceland (hereafter referred to as Eyja) and was collected on the ground immediately after an ash fall event that occurred in Holtsa (~ 4–5 km from the volcano) on 17 April 2010. The ash

sample was sieved at 100 μm to remove large particles that are not representative of the material transported over long distances in the atmosphere (Witham et al. 2005).

The present-day global deposition flux of volcanic ash is not known and annual estimates for the Indian and Southern Oceans are not available. In this study, we used an ash concentration of 25 mg L^{-1}, corresponding to an estimated deposition event of 300 g m^{-2}, that is, equivalent to a 0.2-mm-thick ash deposit (*see* Supporting Information Text S2). This concentration is on the same order of magnitude as the estimates reported for historical eruptions (Olgun et al. 2011) and comparable to previous bioassay experiments in the Atlantic sector of the Southern Ocean (Browning et al. 2014).

Aerosol composition

Total P, Si, and Fe of Pata and Eyja were measured with inductively coupled plasma atomic emission spectrometry (ICP-AES iCAP 6500, Thermo Fisher Scientific) after alkaline fusion (Li-tetraborate/Li-metaborate, 1000°C) and dissolution (HNO_3, 2 mol L^{-1}, ~ 100°C). Total P and Fe were also measured with inductively coupled plasma mass spectrometry (ICP-MS 7500cx, Agilent) after acid digestion (HNO_3 67–69% and HF 40%, Ultrapur) according to Fu (2018). The total N content was quantified with an isotope ratio mass spectrometer (IR-MS Delta V plus, Thermo Fisher Scientific) coupled with a C/N analyzer (Flash EA, Thermo Fisher Scientific).

The median particle diameter was calculated from volume size distribution measured by laser diffraction in ultrapure water (without ultra-sonication to avoid breaking up aggregates). The specific surface area was determined by the Brunauer, Emmet, and Teller gas adsorption method using nitrogen for dust (< 20 μm) and krypton for ash particles (< 100 μm). The mineralogical composition of the crystalline portion of aerosols was measured by quantitative X-ray diffraction according to Nowak et al. (2018), and the proportion of the amorphous phase was determined by adding an internal standard.

Biological and chemical parameters

Primary production

Net CO_2 fixation rates were determined using the ^{13}C-tracer addition method (*see* details in Ridame et al. 2014). Briefly, 1 mL of $NaH_{13}CO_3$ (451 mmol L^{-1} prepared in ultrapure water, 99%, Eurisotop) was added 24 h after the beginning of incubation to 2.3-L polycarbonate bottles to obtain a ~ 10% final enrichment. The bottles were vigorously shaken and put back into on-deck incubators for additional 24 h. After incubation, about 1–2.3 L was gently filtered using precombusted 25-mm Whatman™ GF/F filters and stored at −80°C. It has to be noted that 51.5 mL has also been sampled for cellular abundances and nutrients. The sample filters were dried at 40°C for 48 h before analysis. Carbon in particulate matter and ^{13}C isotopic ratios were quantified using an online continuous flow elemental analyzer (Flash 2000 HT), coupled with an IR-MS (Delta V Advantage via a conflow IV interface from Thermo Fisher Scientific). The atom% excess of the dissolved inorganic carbon (DIC) was calculated using the DIC concentrations measured on board.

Cellular abundance

The cellular abundances of picoeukaryote and nanoeukaryote (< 30 μm), cyanobacteria, and heterotrophic bacteria were determined using a FACS Canto II flow cytometer, equipped with a 488 nm laser and the standard filter setup, according to the protocol detailed in Marie et al. (1999). Briefly, 1.5 mL of seawater was immediately fixed with glutaraldehyde and placed in the dark before being frozen and stored at −80°C prior to analysis. Samples were thawed at room temperature and beads were added as an internal reference. Phytoplankton cells were analyzed (3 min at 100 μL min^{-1}) and populations were discriminated on the basis of their forward and side scatters as well as their phycoerythrin and chlorophyll auto-fluorescence. For heterotrophic cells, samples were stained using SYBR Green-I, incubated in the dark and analyzed (2 min at 50 μL min^{-1}).

Pigments

One to two liters of seawater were filtered onto GF/F filters at initial time and 1 L after 48 h incubation, then immediately placed at −80°C prior to analysis at the SAPIGH analytical platform, Institut de la Mer (IMEV, Villefranche-sur-Mer, France). Filters were extracted at −20°C in 2 mL methanol (100%) containing an internal standard (vitamin E acetate, Sigma©), disrupted by sonication and clarified 1 h later by vacuum filtration through GF/F filters. The extracts were analyzed within 24 h on a complete Agilent© Technologies 1200 series high-performance liquid chromatography (HPLC) system. The general procedure for HPLC pigment analysis, identification and quantification are described in Ras et al. (2008). The sampling at final time at the LNLC stations (2 and 16) could not be carried out due to the insufficient volume of seawater remaining after the sampling of other parameters. Taxonomic pigments were used as size class markers of phototroph groups (picophytoplankton, nanophytoplankton, and microphytoplankton). The chemotaxonomic correspondence of HPLC-determined pigments and the associated size-class came from Uitz et al. (2006), as further presented in the Supporting Information Text S3.

Macronutrients

At initial time, seawater for dissolved Si, DIP, and NO_x determination was filtered on-line from the Go-Flo bottles through acid-cleaned 0.2-μm capsule filters (Sartorius Sartobran-P-capsule 0.45/0.2 μm). At final time (48 h in the abiotic experiments and 1 h in artificial rainwater), samples were filtered on acid-cleaned PALL Supor 0.2-μm polyethersulfone filters (10 mL for dissolved Si, 5 mL for DIP and NO_x). Samples were stored at +5°C (dissolved Si) or −20°C (DIP and NO_x) prior to analysis. Dissolved Si and DIP were

measured with a spectrophotometer (Thermo Fisher Evolution 220) according to the manual colorimetric methods of Grasshoff et al. (1999) and Murphy and Riley (1962), respectively. The concentration of NO_x was measured with the SEAL AutoAnalyzer 3HR, according to Aminot and Kérouel (2007). Ammonium was not measured in this study. The detection limits were 0.03 μmol L^{-1} dissolved Si, 0.03 μmol L^{-1} DIP, and 0.08 μmol L^{-1} NO_x.

Dissolved iron

The same filtration protocol as for macronutrients was used for dissolved Fe samples. After filtration of 30 mL, samples were acidified (0.2% HCl Ultrapur) and stored at +5°C before analysis. Dissolved Fe was measured in seawater by ICP-MS coupled with an automated sample preconcentration system (SeaFAST) according to Wuttig et al. (2019), and in artificial rainwater by ICP-AES (Spectro Arcos). The detection limits were 0.005 and 8.0 nmol L^{-1}, respectively. Due to Fe contamination issues during the analysis of the artificial rainwater samples amended with ash, we estimated the Fe release from ash and the resulting solubility in artificial rainwater ($d\mathrm{Fe}_{\mathrm{ARW}}$) according to a back-calculation of released Fe after the addition of 2% ash-containing artificial rainwater to the abiotic filtered seawater:

$$d\mathrm{Fe}_{\mathrm{ARW}} = \Delta d\mathrm{Fe}_{\mathrm{SW.12h}}/0.02 \quad (1)$$

where $d\mathrm{Fe}_{\mathrm{SW.12h}}$ corresponds to the first available dissolved Fe data point 12 h after addition of artificial rainwater in filtered seawater. This calculated concentration might be biased by secondary Fe release and/or scavenging processes during the first 12 h in the seawater matrix.

Data processing

The nutrient solubility of aerosols ($\%X_{\mathrm{sol}}$, in %) was calculated as follows:

$$\%X_{\mathrm{sol}} = \frac{dX - dX_0}{X_{\mathrm{tot}}} \times 100, \quad (2)$$

where dX and dX_0 are the concentrations of a dissolved nutrient X at final and initial time, and X_{tot} is the amount of X in the added aerosol sample.

The contribution of each phytoplankton size class (x = micro, nano or pico) to the total Chl *a* increase ($\Delta\mathrm{Tchla}_x$, in %) in the nutrient/aerosol treatment (trtm) after 48 h relative to the mean control (ctr) after 48 h was assessed from:

$$\Delta\mathrm{Tchla}_x = \frac{\mathrm{Tchla}_x(\mathrm{trtm.48h}) - \mathrm{Tchla}_x(\mathrm{mean\,ctr.48h})}{\mathrm{Tchla(trtm.48h)} - \mathrm{Tchla(mean\,ctr.48h)}} \times 100. \quad (3)$$

The relative change (RC, in %) in each parameter was calculated as follows:

$$\mathrm{RC\,(in\%)} = (C_{\mathrm{trmt.48h}} - C_{\mathrm{ctr.48h}}) \times 100/C_{\mathrm{ctr.48h}}, \quad (4)$$

with C_{trtm}, the concentration of the parameter at 48 h and C_{ctr}, the mean of the triplicate controls at 48 h.

Statistical analysis

Means (n = 3) at final time in the biotic experiments were compared using a one-way ANOVA followed by a Fisher Least Significant Difference means comparison test. When assumptions for ANOVA were not respected, the tests were performed on the log-transformed data or means were compared using a Kruskal–Wallis test and a post hoc Dunn test. Means of nutrient release for dust and ash in the abiotic experiments were compared using Student's *t*-test. Statistical tests were done using the XLSTAT software. The significance threshold was set to p-value < 0.05.

Results

Characterization of aerosols and nutrient release

Composition of aerosols

The mineralogy and nutrient content of dust and ash materials differ (Table 2): Pata contains more N but less P and Fe than Eyja, and the Si content is similar for both aerosols. The specific surface area of Pata (< 20 μm) is nine times higher than Eyja (< 100 μm). Pata contains twice more clay than Eyja, which has a lower crystallinity. Compared to Saharan dust, which usually contains less than 10% of feldspars (Journet et al. 2008), Pata dust is enriched in magmatic silicate minerals, including albite (18.6 wt.%, Table 2), likely originating from the eruptive products emitted by nearby volcanoes (Simonella et al. 2015).

Abiotic nutrient release

Dry deposition mode. Eyja released more dissolved Fe and DIP than Pata (Table 3a) and similar amounts of dissolved Si, whereas the NO_x release by both aerosols remained undetectable. Compared to ash, dust solubility was more than 10 times and four times higher for Si and Fe, respectively, whereas the released nutrient concentration was equal (Si) or lower (Fe) (Table 3a).

Wet deposition mode. The nutrient release by ash in natural seawater after the addition of 2% artificial rainwater was higher for dissolved Fe and DIP compared to dust (Table 3b). Dissolved Fe and DIP concentrations in seawater that were released after a wet compared to a dry deposition event were similar for Pata and higher for Eyja (Table 3a,b). Surprisingly, the wet deposition induced a decrease in dissolved Si and NO_x concentrations (Table 3b) whereas both aerosols were a source of dissolved Si only in dry deposition mode.

With a 12.5-fold higher particle concentration in artificial rainwater, Eyja released about eight times more dissolved Si and DIP and 18 times more dissolved Fe in artificial rainwater than Pata, whereas the release of NO_x was similar for both aerosols (Table 3c). The solubility of all tested nutrients from Pata was higher relative to Eyja in artificial rainwater.

Table 2. Mineralogical composition and total nutrient content (weight %) of the fine fraction of Pata (< 20 μm) and Eyja (< 100 μm) used in the bioassay and abiotic experiments.

		Desert dust (Pata) Sierra Grande Patagonia	Volcanic ash (Eyja) Eyjafjallajökull Iceland
Mineralogy (%)	Limestones	Calcite 2.9	n.d.
	Acidic rocks	Albite 18.6; quartz 6.2	Albite 23.4; analcime 1.0
	Clays	Illite 20.6; smectite 2.8	Smectite 10.9
	(Hydr)oxides	n.d.	Hematite 0.1
	Amorphous	48.3	63.7
Specific surface area ($m^2\ g^{-1}$)		62.1	7.3
N (%)		0.09 ± 0.01	0.03
P (%)		0.08 ± 0.01	0.18 ± 0.01
Si (%)		25.8	26.47
Fe (%)		4.55 ± 0.23	7.51 ± 0.28

n.d., not detectable.

Table 3. Means of N, P, Si, and Fe release (concentration after the experiment minus initial seawater or artificial rainwater concentrations) and solubility (%) of Pata dust and Eyja ash after 48 h of contact in 0.2-μm filtered surface seawater for particle concentrations of 2 mg L^{-1} Pata dust and 25 mg L^{-1} Eyja ash in (**a**) dry deposition mode (means at the five stations) in filtered seawater and (**b**) in wet deposition mode (HNLC-11 only). (**c**) Nutrient release and solubility after 1 h of contact with artificial rainwater at HNLC-11 for particle concentrations of 100 mg L^{-1} Pata dust and 1250 mg L^{-1} Eyja ash.

(a)	Released concentration	NO_x, μmol L^{-1}	DIP, μmol L^{-1}	dSi, μmol L^{-1}	dFe, nmol L^{-1}
	Pata	n.d.	n.d.	0.2 ± 0.2^a	0.7 ± 0.6^a
	Eyja	n.d.	0.10 ± 0.05	0.3 ± 0.1^a	3.8 ± 1.6^b
	Solubility	**N, %**	**P, %**	**Si, %**	**Fe, %**
	Pata	n.d.	n.d.	1.25 ± 0.52^a	0.041 ± 0.035^a
	Eyja	n.d.	6.8 ± 3.4	0.11 ± 0.05^b	0.011 ± 0.005^b
(b)	**Released concentration**	**NO_x, μmol L^{-1}**	**DIP, μmol L^{-1}**	**dSi, μmol L^{-1}**	**dFe, nmol.L^{-1}**
	Pata	−0.5 ± 0.0	n.d.	-2.2 ± 0.6^a	0.7 ± 0.3^a
	Eyja	−0.4 ($n = 1$)	0.4 ± 0.0	-1.2 ± 0.3^b	9.0 ± 0.1^b
	Solubility	**N, %**	**P, %**	**Si, %**	**Fe, %**
	Pata	< 0	n.d.	< 0	0.041 ± 0.017^a
	Eyja	< 0	29.7 ± 2.2	< 0	0.027 ± 0.000^a
(c)	**Released concentration**	**NO_x, μmol L^{-1}**	**DIP, μmol L^{-1}**	**dSi, μmol L^{-1}**	**dFe, nmol.L^{-1}**
	Pata	0.15 ± 0.03^a	1.65 ± 0.05^a	1.92 ± 0.10^a	47.2 ± 0.9^a
	Eyja	0.11 ± 0.01^a	15.41 ± 0.60^b	15.41 ± 0.24^b	$856.7 \pm 35.4^{b,*}$
	Solubility	**N, %**	**P, %**	**Si, %**	**Fe, %**
	Pata	2.18 ± 0.50^a	60.6 ± 1.8^a	0.21 ± 0.01^a	0.058 ± 0.001^a
	Eyja	0.38 ± 0.02^b	20.8 ± 0.8^b	0.13 ± 0.00^b	$0.051 \pm 0.002^{b,*}$

dSi, dissolved Si; dFe, dissolved Fe; n.d., not detectable.
*Fe release and solubility of Eyja ash in ARW were estimated according to Eq. 1
Only detectable nutrient releases (mean concentrations after 48 h in the dust/ash treatments significantly different from means in the control at t-ini, $p < 0.05$) are shown. Means that are not significantly different between dust and ash treatment for each element are labeled with the same superscript letter "a" or "b" ($p > 0.05$). Negative dissolution values express a decrease of NO_x or dissolved Si in seawater after artificial rainwater addition.

Initial features of the incubated seawater

The surface seawater at the studied stations had contrasted physico–chemical and biological features (Table 4), displaying a southward decrease in sea surface temperature and salinity and an increase in macronutrients. At the LNLC stations (2 and 16), the molar NOx/DIP ratio was notably lower than the Redfield ratio (16/1, Redfield 1934). The low dissolved Si concentrations at HN-LSi-LC-14 and Kerguelen-A3 led to molar dissolved Si/NO_x ratios lower than the optimal ratio for diatoms (Si/N = 1.12 ± 0.33, Brzezinski 1985), whereas the

Table 4. Initial physico-chemical and biological properties of the surface seawater used for the microcosm experiments. Mean nutrient concentration ± standard deviation of replicates ($n = 3$). Phytoplankton size-fractions according to Uitz et al. (2006): pico: 0.4–2 μm, nano: 2–10 μm, micro: > 10 μm.

Station	2	16	14	A3	11
Zone	STZ	STZ	SAZ	AZ	AZ
Region	LNLC	LNLC	HN-LSi-LC	Kerguelen	HNLC
Latitude, °S	29.97	35.00	42.49	50.64	56.50
Longitude, °E	54.11	73.47	74.90	72.05	62.99
Sampling date	12 Jan 2019	05 Feb 2019	30 Jan 2019	27 Jan 2019	23 Jan 2019
Temperature,°C	24.6	22.0	12.8	4.4	2.1
Salinity	35.47	35.48	34.49	33.83	33.83
NO_x, μM	< DL	< DL	8.11 ± 0.41	20.60 ± 0.77	25.25 ± 0.01
DIP, μM	0.03 ± 0.00	0.09 ± 0.01	0.65 ± 0.02	1.04 ± 0.05	1.58 ± 0.16
dSi, μM	1.79 ± 0.05	1.61 ± 0.05	0.99 ± 0.00	1.59 ± 0.06	16.67 ± 0.15
NO_x/DIP	< 2.7	< 0.9	12.5	19.8	16.0
dSi/NO_x	> 22.4	> 20.1	0.12	0.08	0.67
dFe, nM	0.54 ± 0.12	0.37	0.39	0.35 ± 0.13	0.27 ± 0.02
Synechococcus, cells mL^{-1}	1703	< DL	13,620	349	< DL
Picoeukaryotes, cells mL^{-1}	452	882	5786	401	571
Nanoeukaryotes, cells mL^{-1}	339	209	2798	644	1176
Heterotrophic bacteria, cells mL^{-1}	655,782	547,742	1,310,728	615,636	441,028
PP, mg C m^{-3} d^{-1}	2.78	3.67	26.7	54.42	7.24
Tchla, μg L^{-1}	0.085	0.049	0.603	1.40	0.157
% Micro	13	10	28	92	45
% Nano	24	28	54	7	54
% Pico	63	62	18	1	2

STZ, Subtropical Zone; SAZ, Subantarctic Zone; AZ, Antarctic Zone; dSi, dissolved Si; dFe, dissolved Fe; PP, primary production; Tchla, total Chl *a*; < DL, below detection limit.

nutrient ratio at HNLC-11 was closer to the optimal value (Table 4). The NO_x and DIP concentrations were the highest at the stations within the Antarctic Zone (A3 and 11), whereas the highest dissolved Fe concentration (0.54 nmol L^{-1}) was recorded at LNLC-2 and the lowest at HNLC-11 (Table 4).

The LNLC stations were characterized by the lowest phytoplanktonic biomass, dominated by picophytoplankton. The PP at HN-LSi-LC-14 was over seven times higher than at the LNLC stations, and the algal biomass was dominated by nanophytoplankton (mainly nanoflagellates and chromophytes, data not shown). The highest PP and Tchla were recorded at Kerguelen-A3 where the phytoplankton community was largely dominated by microphytoplankton (Table 4) and mainly diatoms. The PP at HNLC-11 was eight times lower relative to Kerguelen-A3, and the phytoplankton community was co-dominated by nanoplankton and microplankton.

Biological responses

Primary production

Except at LNLC-16, the PP significantly increased after dust or ash additions (Fig. 2), as well as after a Fe or Si addition. The highest increase was observed at Kerguelen-A3 (+105% for aerosol additions). No significant difference was observed after Fe addition alone or in combination with Si. At the LNLC stations, N and NP additions led to the highest PP increase.

Cellular abundances

Aerosol additions had a contrasted impact on cellular abundances (< 30 μm) according to the phytoplankton class, the aerosol type and the station (Fig. 3). In the LNLC area, picoeukaryotes were more stimulated by dust than by ash addition at LNLC-2 (+96% and +50%, respectively), whereas only ash stimulated their growth at LNLC-16 (+38%, Fig. 3 a,d). Additions of both aerosol types had a similar effect on *Synechococcus* (∼ +70% at Sta. 2, Fig. 3c), and no impact on nanoeukaryotes at these stations.

At HN-LSi-LC-14, ash addition enhanced picoeukaryote abundance (+ 32%, Fig. 3f), whereas dust stimulated nanoeukaryotes and heterotrophic bacteria (+44%, Fig. 3j and +36%, Supporting Information Fig. S2). On the contrary, at Kerguelen-A3, dust and ash triggered similar responses in phytoplanktonic abundances, which increased by 140%, 75%, and 40% for *Synechococcus*, picoeukaryote and nanoeukaryote, respectively (Fig. 3i–k). Moreover, ash also stimulated heterotrophic bacteria (+30%, Supporting Information Fig. S2). At HNLC-11, a wet and dry addition of dust or ash induced only

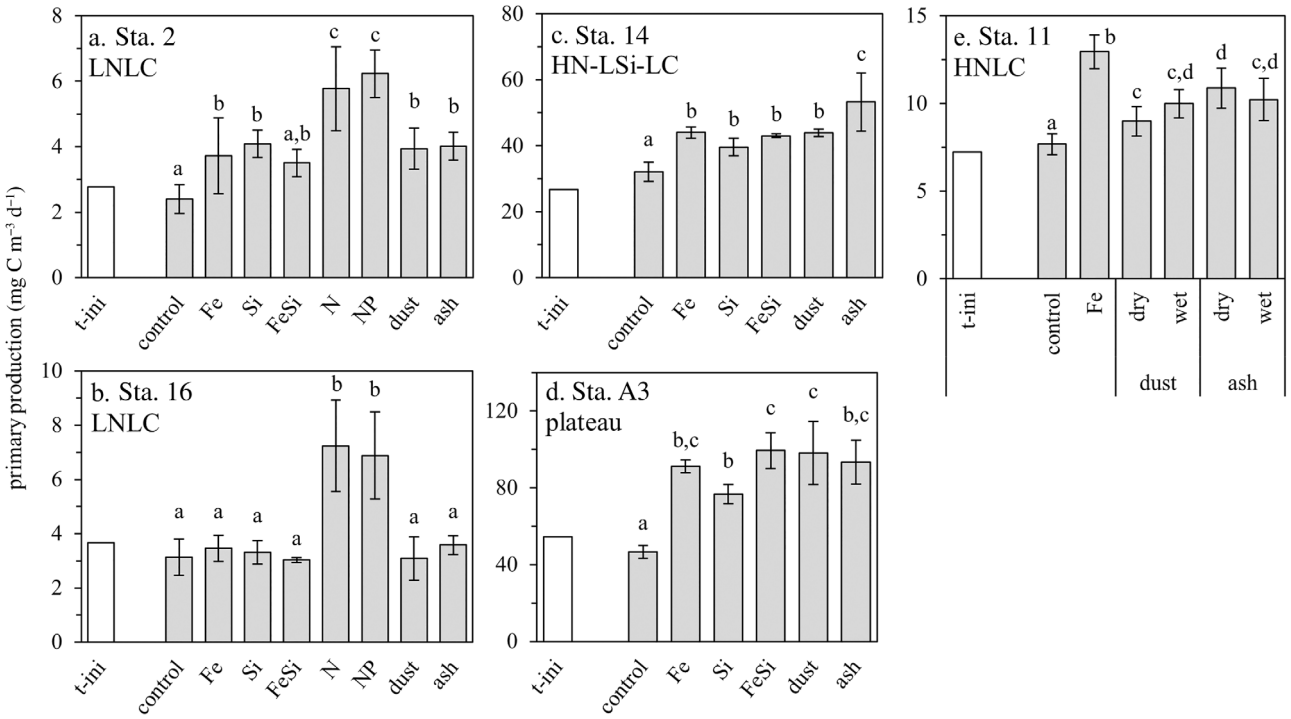

Fig. 2. Primary production (PP, mg C m^{-3} d^{-1}) at the beginning of the experiment (t-ini, white bars) and after 48 h of incubation for each treatment at the stations LNLC Sta. 2 (**a**) and Sta. 16 (**b**), HN-LSi-LC Sta. 14 (**c**), plateau Sta. A3 (**d**) and HNLC Sta. 11 (**e**). Error bars indicate standard deviation of triplicates. Means that are not significantly different ($p > 0.05$) are labeled with the same letter within a station.

a stimulation of the nanoeukaryote abundance (~ +40%), similar to that after nutrient addition (Fig. 3m).

Pigments

The addition of aerosols or nutrients induced an increase in both Tchla and fucoxanthin concentrations relative to the controls at t48 h at Stas. 14, A3, and 11 (Fig. 4). At Kerguelen-A3, these increases were higher after ash compared to dust addition (Fig. 4b,e), whereas they were similar at HN-LSi-LC-14 and HNLC-11.

At these three stations, the addition of aerosols or nutrients benefited mostly microphytoplankton, and in particular diatoms, which sustained from 52 up to 100% of the Tchla increase (Fig. 5). The community structure was thus modified at these stations (Supporting Information Fig. S1). Interestingly at HN-LSi-LC-14, although the respective contribution of diatoms and dinoflagellates to Tchla were quite similar in the control at t48 h (~ 15%, Supporting Information Fig. S1 a), the diatom contribution doubled after ash and Si additions, whereas that of dinoflagellates did not change.

Discussion

The abiotic experiments (Table 3) demonstrated that the dust and ash samples released significant amounts of Fe and Si to seawater. However, none of these materials acted as a source of NOx in seawater (Table 3). These findings are consistent with previous abiotic studies performed with Saharan dust (Mills et al. 2004; Ridame et al. 2014) and ash specimens (Jones and Gislason 2008; Browning et al. 2014). Arguably, Pata and Eyja relieved or reduced the ambient Fe and/or Si limitations of PP in the Southern Ocean but were not able to alleviate the N limitation in the Southern Indian Ocean (Fig. 2).

Moreover, we cannot exclude a bias caused by grazing, as we did not remove zooplankton predators from the natural plankton community prior to the experiments. However, the responses are interpreted relative to the control, thus we assume that the potential bias should be of the same magnitude in control as in the treatments.

Phytoplankton response

LLNLC stations

Interestingly, the phytoplankton response to aerosol additions was contrasted between the LNLC stations: aerosols led to a significant PP increase at the western LNLC-2, whereas no change was observed at the eastern LNLC-16. This difference can be related to the initial nutrient limitation: the eastern station was N-limited, as previously shown by Twining et al. (2019), whereas the PP in the western station was N-, Fe-, and Si-limited (Fig. 2a), and dust and ash stimulated significantly the picoeukaryotes and *Synechococcus* abundances at LNLC-2. The detection of *Prochlorococcus*-specific pigments at

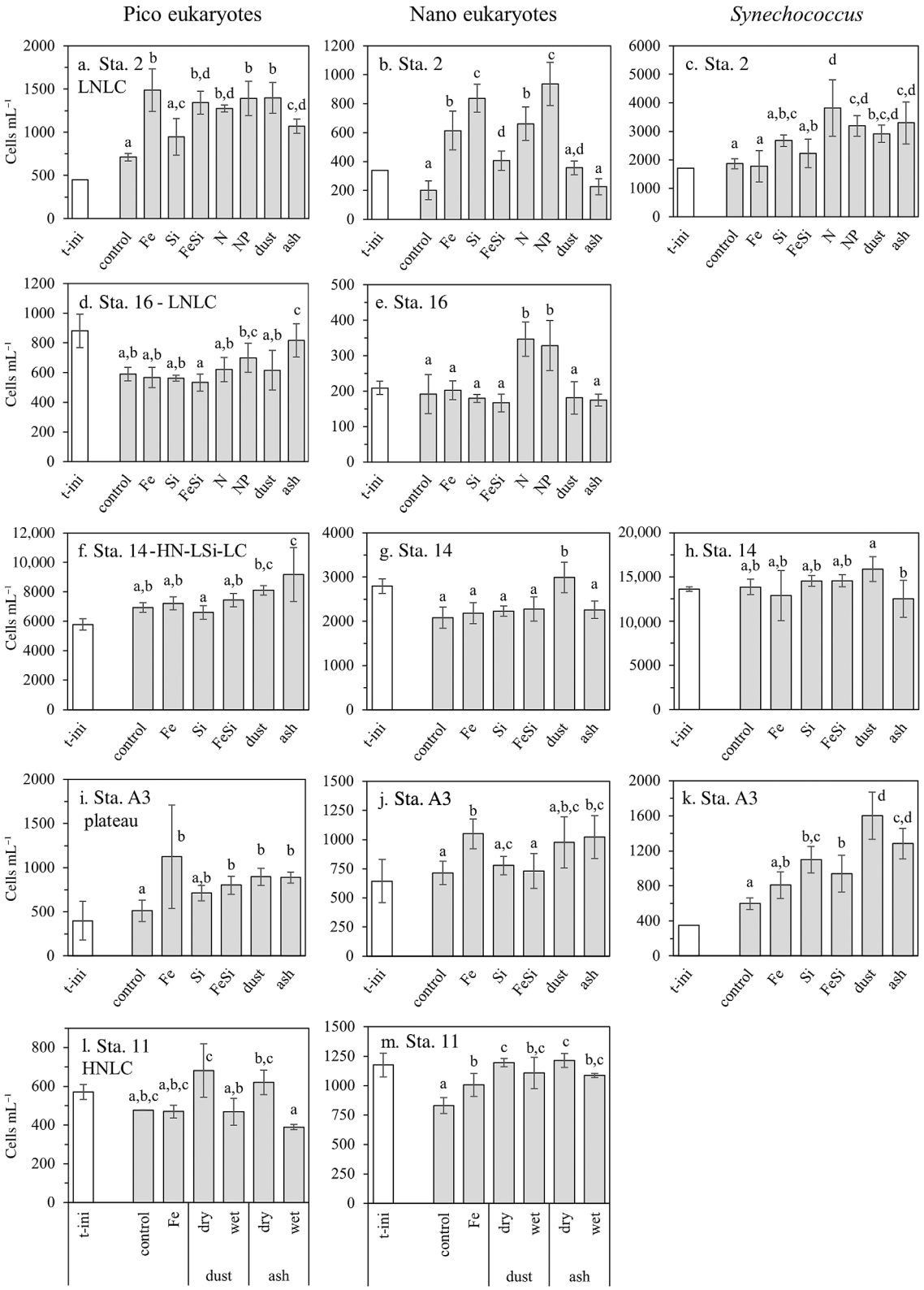

Fig. 3. Cell abundance (cells mL^{-1}) of picoeukaryotes (**a**,**d**,**f**,**i**,**l**), nanoeukaryotes (**b**,**e**,**g**,**j**,**m**), and *Synechococcus* (**c**,**h**,**k**) at the beginning of the experiment (t-ini, white bars) and after 48 h of incubation for each treatment at the LNLC Sta. 2 (**a**–**c**) and 16 (**d**–**e**), HN-LSi-LC Sta. 14 (**f**–**h**), Kerguelen Sta. A3 (**i**–**k**), and HNLC Sta. 11 (**l**–**m**). Error bars indicate standard deviation of triplicates. Means that are not significantly different ($p > 0.05$) are labeled with the same letter within a station.

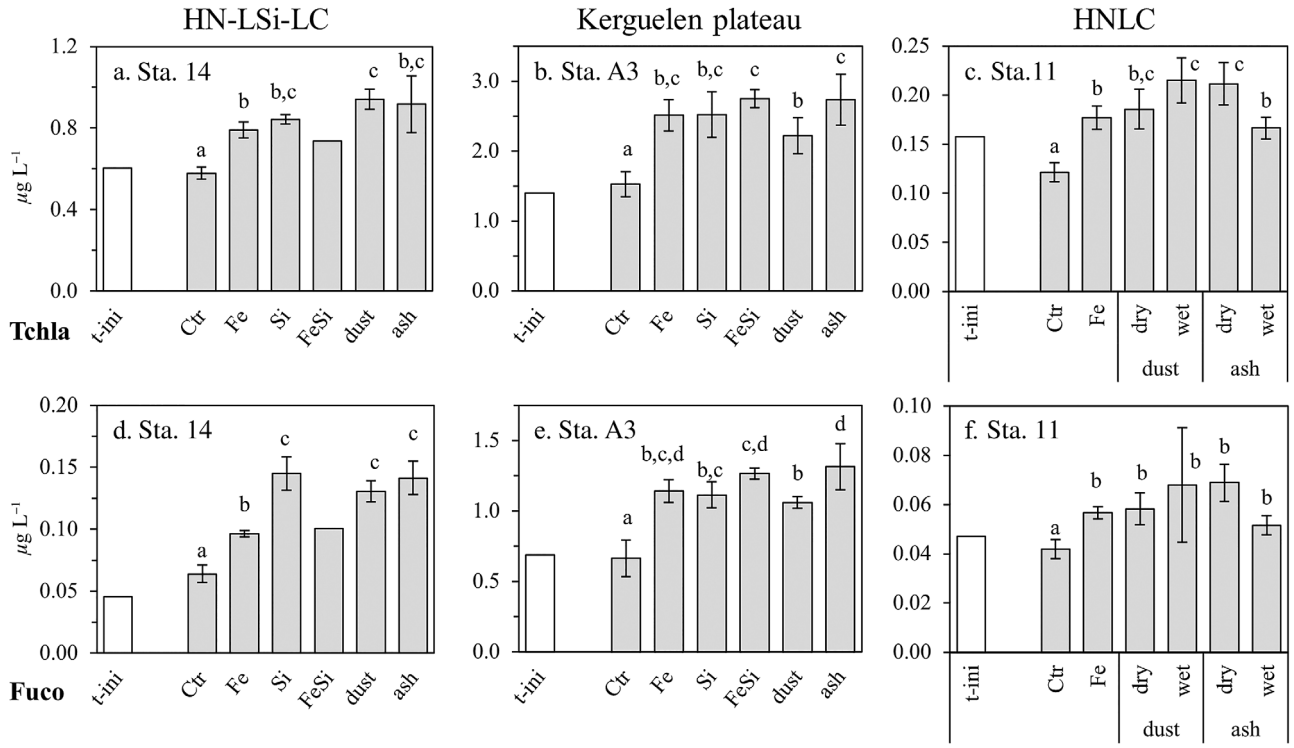

Fig. 4. Pigment concentration (μg L^{-1}) of total chlorophyll *a* (**a**–**c**) and fucoxanthin (**d**–**f**) at the beginning of the experiment (t-ini, white bars) and after 48 h of incubation for each treatment at HN-LSi-LC Sta. 14 (**a**,**d**), plateau Sta. A3 (**b**,**e**) and HNLC Sta. 11 (**c**,**f**). Error bars indicate standard deviation of triplicates. FeSi treatment at Sta. 14 is not included in statistics, due to $n = 1$. Means that are not significantly different ($p > 0.05$) are labeled with the same letter within a station.

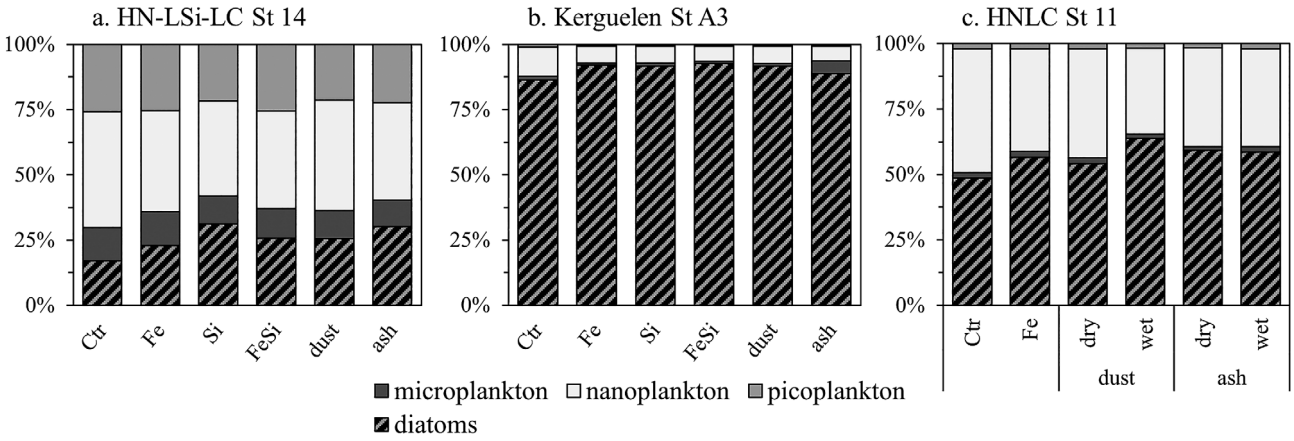

Fig. 5. Size depending relative contribution to Tchla increase (%) after 48 h of incubation for each treatment relative to control at HN-LSi-LC Sta. 14 (**a**), Kerguelen Sta. A3 (**b**) and HNLC Sta. 11 (**c**), with microplankton (dark), nanoplankton (light), and picophytoplankton (median gray). Diatom contribution within the microplankton size fraction is dashed.

initial time at these stations (16–30 ng L^{-1} of divinyl-Chl *a*) without flow cytometric detection might indicate that the cell fluorescence was too low to be detected by cytometry. As pigment content could not be analyzed at final time at these stations, we cannot conclude on the response of microphytoplankton to the nutrient/aerosol additions.

Despite a generally low seasonality within the Subtropical Zone, the 3-week difference in the sampling time between the western and eastern stations (Table 4) may contribute to the differences in the initial nutrient dynamics and the phytoplankton community structure, leading to different biological responses. Moreover, the community at the western station

may be influenced by the South East Madagascar Bloom (Fig. 1a), explaining an initial algal biomass twice as high at the western compared to the eastern station which lies in more typical oligotrophic waters. Moreover, heterotrophic bacteria (stimulated after FeSi and NP additions at the eastern LNLC-16, Supporting Information Fig. S2b) may compete for nutrient uptake and thus explain the limited autotroph response, as already observed in the oligotrophic tropical Atlantic (Marañón et al. 2010).

HN-LSi-LC station

The about 10 times lower dissolved Si/NO_x ratio compared to the optimal ratio for diatoms (Si/N = 1.12, Brzezinski 1985) suggests a potential Si limitation of the diatom activity at HN-LSi-LC-14, as demonstrated by PP increase (Fig. 2c) and previous studies in the Indian (Sedwick et al. 2002) and Australian (Hutchins et al. 2001) sectors of the Subantarctic Zone. Diatoms responded similarly to dust, ash and Si additions (Fig. 4d), indicating that the diatom Si-limitation could be alleviated by aerosol input. Because of a potential Fe contamination of the Si solution (Supporting Information Text S1), these similar responses may also indicate that dust and ash were capable of mitigating a potential co-limitation of diatoms by Si and Fe. In the abiotic experiment, a dry deposition of dust or ash released around 0.3 μmol L^{-1} dissolved Si (Table 3a), which indicates that the initial Si-limitation could be eased with a relatively low absolute release, representing +20 to +33% of the initial stock. Despite the low contribution of diatoms to the initial biomass, their strong development after aerosol addition explained roughly half of the increase in Tchla (+39% and +60% for dust and ash, respectively, Fig. 6), as already reported within the Australian Subantarctic Zone after Fe and/or Si additions (Hutchins et al. 2001). Thus, picooeukaryote and nanoeukaryote may be less competitive than diatoms for new nutrient uptake.

The *Synechococcus* abundance, which was the highest at this station, did not change after new nutrient supply. This suggests that this species was either not nutrient-limited and/or could not benefit from this addition and/or was subjected to important grazing, as previously described by Hutchins et al. (2001) in the Subantarctic Zone of the Australian sector of the Southern Ocean.

HNLC station

The PP of HNLC-11 was mainly Fe-limited, despite a higher surface dissolved Fe concentration in this study compared to published data from the same ocean area and season (KEOPS-1, January–February 2005) (Blain et al. 2008). The measured dissolved Fe concentration was, however, comparable to the same stations during austral spring (KEOPS-2, October–November 2011) (Bowie et al. 2015), as well as to the central Indian and Atlantic sectors of the Southern Ocean (Chever et al. 2010; Grand et al. 2015).

At this station, we compared the phytoplankton response to both dry and wet deposition modes, well known to influence nutrient solubility (Duggen et al. 2010; Chester and Jickells 2012). Dust and ash, as well as Fe addition led to a stimulation of PP and Tchla, confirming that dry and wet depositions of dust and ash were a significant source of bioavailable Fe for phytoplankton and more specifically for diatoms. This confirms also the results from the abiotic experiment (Table 3) and the previous studies in HNLC areas (Langmann et al. 2010; Browning et al. 2014; Mélançon et al. 2014). Interestingly, in the Atlantic sector of the Southern Ocean, Trimborn et al. (2017) found no biological response after four to eight times lower Fe and dust additions than in our study, suggesting that there is a required dissolved Fe threshold to observe phytoplankton response in the severely Fe-limited Southern Ocean (Boyd et al. 2010).

Kerguelen plateau station

Aerosol additions triggered a PP increase similar to that observed after Fe and/or Si additions, indicating a Fe and Si growth limitation that can be explained by the low dissolved Si concentration at Kerguelen-A3 (10.5 times lower than at HNLC-11) and the season in late summer (end of January) at the end of the diatom bloom (Timmermans et al. 2008; Closset et al. 2014).

The plateau station was initially dominated by diatoms which also explain the major increase in Tchla (Fig. 6) after an aerosol/nutrient deposition. Surprisingly, *Synechococcus* abundance increased after Si addition. Silicon is not recognized as a nutrient for cyanobacteria, but Si bioaccumulation within picocyanobacteria such as *Synechococcus* has already been observed in the West Pacific and Sargasso Sea as well as in cultured strains (Baines et al. 2012; Krause et al. 2017; Wei et al. 2021). However, to our knowledge, such silicifying *Synechococcus* have not yet been detected near the Kerguelen Islands.

Surprisingly, the most productive station Kerguelen-A3 was the station with the highest relative change in PP after aerosol/nutrient addition (~ +100%), whereas the increase in PP was lower at HNLC-11 (~ +46%) (Fig. 2d,e). One hypothesis to explain this different intensity of the biological response may be a precondition of the Kerguelen plateau phytoplankton community to frequent nutrient supply from the sediment, potentially accelerating the response to aerosol/nutrient addition. The more intense response may also be related to the different composition of the natural phytoplanktonic community, as Kerguelen-A3 was dominated by bloom-enabling diatoms, compared to the surrounding open ocean HNLC waters co-dominated by nanoplankton and diatoms (Fig. 6). The HNLC population is acclimated to Fe limiting concentrations, and it may require a longer period of time to reach maximal biological response. Thus, the short time scale of our experiments (48 h) may not have been sufficient to overcome the lag phase. A similar phenomenon has been described by Moore et al. (2007) during the CROZEX in situ Fe addition experiment in the same sector of the Southern Ocean, where the biological response occurred mostly after

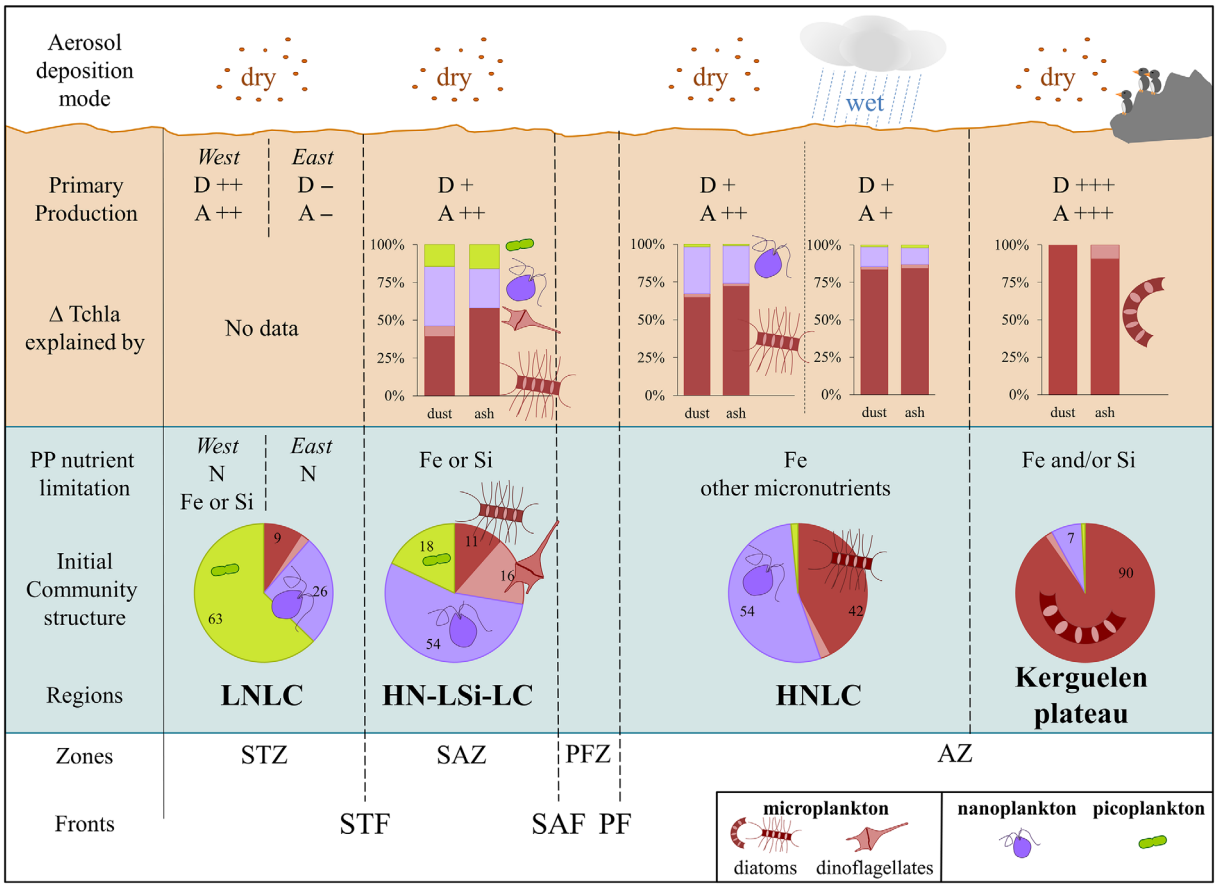

Fig. 6. Schematic representation of the biological response of phytoplankton communities after dry or wet dust (D) or ash (A) deposition to the sea surface within different biogeochemical regions of the South Indian Ocean and Southern Ocean. The top part of the figure (orange box) shows the phytoplankton response to aerosol deposition (PP and ΔTchla), while the bottom part (blue box) represents the initial conditions prior to deposition (nutrient limitation and phytoplankton structure). Primary production is expressed in relative change (%), as follows: +++ above 100%; ++ above 50%; + below 50%;– no significant change compared to control. ΔTchla shows the contribution (%) of different phytoplankton classes explaining the global increase in Tchla. The community composition (initial and final) is based on the pigment signature, with red: microplankton (dark: diatoms and light: dinoflagellates), purple: nanoplankton, and green: picoplankton. The graphic concerns solely the surface layer and response after 48 h, regardless of depth and particle sinking. The represented taxa are representative for the Southern Ocean: microplankton: *Eucampia* and *Chaetoceros* (coastal and open ocean diatoms, respectively), *Ceratium* (dinoflagellate); nanoplankton: *Phaeocystis* (haptophyte); pico-plankton: *Synechococcus* (cyanobacteria). Zones and fronts (from North to South): Subtropical Zone and Front (STZ and STF); Subantarctic Zone and Front (SAZ and SAF); Polar Front Zone and Polar Front (PFZ and PF); and Antarctic Zone (AZ).

3 d of incubation. Similarly, Timmermans et al. (2008) observed a twice longer lag phase (12 vs. 6 days) in their HNLC phytoplankton experiment compared to the Kerguelen plateau phytoplankton community during translocation experiments.

Influence of physico–chemical parameters on nutrient release by aerosols

Aerosol type: Importance of origin and mineralogy

Surprisingly, the biological response induced by a dry deposition of the two aerosol types was generally very similar, independently of the studied biogeochemical area except for stations HNLC-11 and HN-LSi-LC-14 (*see* "Discussion" section). We observed identical Si release despite different particle concentrations, a result reflecting a significantly higher Si solubility in dust than ash (Table 3a), that could be (partly) due to higher specific surface area, combined to the differences in mineralogy (Table 2) with variable solubilities and dissolution kinetics (Geisen 2021).

At LNLC-2 and Kerguelen-A3, the PP increase occurred regardless of the nature of the added aerosol. At these stations, no significant difference in PP was observed between dust, ash and Fe additions, suggesting that the Fe released by aerosols may be bioavailable and sufficient to relieve the ambient Fe-limitation. It is likely that the Fe-limitation was not very severe at these stations and that the mean 0.7 nmol L^{-1} dissolved Fe provided by dust deposition was sufficient to reach the maximal response rate of cell division and PP. The LNLC community remained nonetheless N-limited.

In contrast, at HNLC-11 and HN-LSi-LC-14, a dry deposition of ash triggered around twice more PP than a dry deposition of dust ($p < 0.05$), which likely resulted from the higher Fe supply from the ash addition compared to the dust

(Table 3). At HNLC-11, the greater PP response after the addition of ash compared to nutrients/dust may also indicate that other micronutrients (such as manganese; Frogner et al. 2001) released by Eyja ash could relieve additional PP limitations. At HNLC-11, Fe addition induced more PP increase than aerosols, which suggests that unknown synergistic effects between the released elements weakened the positive effect of Fe release (Paytan et al. 2009; Hoffmann et al. 2012) or that the local communities were differently influenced by the direct nutrient supply of the Fe solution compared to the potentially more gradual nutrient dissolution from the aerosols.

Deposition mode

The addition of dust and ash in both dry and wet deposition modes performed at HNLC-11 enabled to compare the influence of the initial contact medium on nutrient release, with varying pH (8.1 and 4.7 for seawater and rainwater, respectively) and ionic charge, as well as the presence of dissolved organic matter in natural seawater. Iron dissolution of dust particles is known to decrease with increasing pH (Desboeufs et al. 1999; Journet et al. 2008; Paris et al. 2011), whereas organic matter, and in particular the presence of Fe-binding ligands, increases Fe solubility and bioavailability in seawater (Wagener et al. 2008; Hassler et al. 2011; Paris and Desboeufs 2013). Thus, nutrient release may be impacted by a complex array of antagonistic parameters.

In our abiotic experiment, the highest Fe solubility for dust and ash occurred in artificial rainwater (Table 3c). Moreover, although the deposition mode did not significantly influence the dissolved Fe release from dust to seawater (0.7 nmol L^{-1} after 48 h of contact, Table 3a,b), ash released 2.4 times more Fe to seawater in wet compared to dry deposition mode (9.0 and 3.8 nmol L^{-1}, respectively). The addition of 2% artificial rainwater to seawater should theoretically release 0.94 and 17.1 nmol L^{-1} dissolved Fe to seawater after wet dust or ash deposition. The difference between the measured wet deposition and theoretical release (significant only for ash deposition) may indicate that Fe adsorption and/or precipitation processes dominate over secondary Fe dissolution in seawater. Moreover, the quality and quantity of organic matter in the seawater may explain the high variability in Fe solubility, as previously reported (Wagener et al. 2008; Bressac and Guieu 2013).

A wet deposition of either aerosol induced a moderate increase in PP ($\sim$ +40%, Fig. 2e), intermediate between the higher impact of dry ash deposition (+ 50%) and a lower reaction after a dry dust deposition (+ 24%). Equally, Tchla and fucoxanthin increases were independent of the dust deposition mode, consistent with the equal abiotic Fe dissolution, indicating that the Fe released by both mechanisms was equally bioavailable.

Conclusions

Our results from incubation experiments demonstrate that the desert dust and volcanic ash materials, despite contrasted mineralogical and chemical composition released significant amounts of Fe and Si to seawater in the Indian and Southern Oceans. A representative deposition of both dust and ash was sufficient to trigger a phytoplankton response, mainly driven by a stimulation of the diatom community (Fig. 6). Ash addition elicited an equivalent or greater biological response than dust, depending on the severity of the initial Fe-limitation. However, neither the tested dust nor the ash was a significant source of NOx.

After dust or ash additions, the maximum relative and absolute increase in PP was observed at the most productive station over the Kerguelen Plateau, whereas the lowest relative response was found at the HNLC station despite similar nutrient limitations. We hypothesize that acclimation of the ambient phytoplankton community to either frequent nutrient supply through winter mixing, causing a rapid doubling of the PP or, on the contrary, scarce nutrient supply induced an initial lag phase and thus a longer time laps before reaching a maximum response. Moreover, the HNLC phytoplankton community was only slightly affected by a wet rather than a dry deposition of aerosols, as the dominant diatom community responded equally to both deposition modes.

Future work should focus on the dissolution and possible bioavailability of other trace elements such as manganese and cobalt dissolved from dust and ash particles (Fishwick et al. 2018) as these may also limit phytoplankton growth in the open ocean (Mackey et al. 2012; Perron et al. 2020). Since the seasonal and spatial variability of organic matter concentration in surface seawater may impact nutrient dissolution and scavenging processes (de Leeuw et al. 2014), its influence on the response of phytoplankton to aerosol additions should also be investigated (Bressac and Guieu 2013; Hernández-Ruiz et al. 2020).

Moreover, nutrient bioavailability in the Southern Ocean may be disturbed in the future, according to climate change predictions (Deppeler and Davidson 2017). Predicted changes in the Southern Ocean for 2100 include increased sea surface temperature, and around twice higher CO_2 concentrations leading to ocean acidification. Although dust deposition to the Southern Ocean has doubled during the 20th century (McConnell et al. 2007) and is thought to further increase, the pycnocline and mixed layer depth will become shallower (Deppeler and Davidson 2017). Thus, more aerosols should dissolve in a lower volume of warmer, fresher and more acidic surface ocean, increasing particle concentration and nutrient release (Deppeler and Davidson 2017). Thus, further research is needed to better constrain the evolution of aerosol load and associated nutrient bioavailability in a changing ocean.

Data availability statement

The dataset is available at the address: https://www.seanoe.org/data/00696/80825/

References

Aminot, A., and R. Kérouel. 2007. Dosage automatique des nutriments dans les eaux marines: méthodes en flux continu., P. 188. In Ifremer-Quae [ed.]. Méthodes d'analyses en milieu marin. IFREMER. ISBN: 13 978-2-7592-0023-8

Ardyna, M., and others. 2019. Hydrothermal vents trigger massive phytoplankton blooms in the Southern Ocean. Nat. Commun. **10**: 2451. doi:10.1038/s41467-019-09973-6

Ayris, P., and P. Delmelle. 2012. Volcanic and atmospheric controls on ash iron solubility: A review. Phys. Chem. Earth **45–46**: 103–112. doi:10.1016/j.pce.2011.04.013

Baines, S., B. S. Twining, M. A. Brzezinski, J. Krause, S. Vogt, D. Assael, and H. McDaniel. 2012. Significant silicon accumulation by marine picocyanobacteria. Nat. Geosci. **5**: 886–891. doi:10.1038/ngeo1641

Blain, S., and others. 2007. Effect of natural iron fertilization on carbon sequestration in the Southern Ocean. Nature **446**: 1070–1074. doi:10.1038/nature05700

Blain, S., G. Sarthou, and P. Laan. 2008. Distribution of dissolved iron during the natural iron-fertilization experiment KEOPS (Kerguelen Plateau, Southern Ocean). Deep Sea Res. Part II Top. Stud. Oceanogr. **55**: 594–605. doi:10.1016/j.dsr2.2007.12.028

Bowie, A. R., and others. 2015. Iron budgets for three distinct biogeochemical sites around the Kerguelen Archipelago (Southern Ocean) during the natural fertilisation study, KEOPS-2. Biogeosciences **12**: 4421–4445. doi:10.5194/bg-12-4421-2015

Boyd, P. W., and others. 2007. Mesoscale iron enrichment experiments 1993–2005: Synthesis and future directions. Science **315**: 612–617. doi:10.1126/science.1131669

Boyd, P. W., D. S. Mackie, and K. A. Hunter. 2010. Aerosol iron deposition to the surface ocean—Modes of iron supply and biological responses. Mar. Chem. **120**: 128–143. doi:10.1016/j.marchem.2009.01.008

Bressac, M., and C. Guieu. 2013. Post-depositional processes: What really happens to new atmospheric iron in the ocean's surface? Global Biogeochem. Cycl. **27**: 859–870. doi:10.1002/gbc.20076

Browning, T. J., H. A. Bouman, G. M. Henderson, T. A. Mather, D. M. Pyle, C. Schlosser, E. M. S. Woodward, and C. M. Moore. 2014. Strong responses of Southern Ocean phytoplankton communities to volcanic ash. Geophys. Res. Lett. **41**: 2851–2857. doi:10.1002/2014GL059364

Brzezinski, M. A. 1985. The Si:C:N ratio of marine diatoms: Interspecific variability and the effect of some environmental variables. J. Phycol. **21**: 347–357. doi:10.1111/j.0022-3646.1985.00347.x

Chester, R., and T. D. Jickells. 2012. The transport of material to the oceans: The atmospheric pathway, p. 52–82. *In* Marine geochemistry. John Wiley & Sons Ltd.

Chever, F., E. Bucciarelli, G. Sarthou, S. Speich, M. Arhan, P. Penven, and A. Tagliabue. 2010. Physical speciation of iron in the Atlantic sector of the Southern Ocean along a transect from the subtropical domain to the Weddell Sea Gyre. J. Geophys. Res. Ocean **115**: 1–15. doi:10.1029/2009JC005880

Closset, I., M. Lasbleiz, K. Leblanc, B. Quéguiner, A. J. Cavagna, M. Elskens, J. Navez, and D. Cardinal. 2014. Seasonal evolution of net and regenerated silica production around a natural Fe-fertilized area in the Southern Ocean estimated with Si isotopic approaches. Biogeosciences **11**: 5827–5846. doi:10.5194/bg-11-5827-2014

Conway, T. M., E. W. Wolff, R. Rothlisberger, R. Mulvaney, and H. E. Elderfield. 2015. Constraints on soluble aerosol iron flux to the Southern Ocean at the Last Glacial Maximum. Nat. Commun. **6**: 7850. doi:10.1038/ncomms8850

de Leeuw, G., and others. 2014. Ocean–atmosphere interactions of particles. *In* P. S. Liss and M. T. Johnson [eds.], Ocean–atmosphere interactions of gases and particles. Springer.

Deppeler, S. L., and A. T. Davidson. 2017. Southern Ocean phytoplankton in a changing climate. Front. Mar. Sci. **4**: 40. doi:10.3389/fmars.2017.00040

Desboeufs, K. V., R. R. Losno, S. Cholbi, F. Vimeux, and S. Cholbi. 1999. The pH-dependent dissolution of wind-transported Saharan dust. J. Geophys. Res. Atmos. **104**: 21287–21299. doi:10.1029/1999JD900236

Dugdale, R. C., F. P. Wilkerson, and H. J. Minas. 1995. The role of a silicate pump in driving new production. Deep Sea Res. Part I Oceanogr. Res. Pap. **42**: 697–719. doi:10.1016/0967-0637(95)00015-X

Duggen, S., N. Olgun, P. Croot, L. J. Hoffmann, H. Dietze, P. Delmelle, and C. Teschner. 2010. The role of airborne volcanic ash for the surface ocean biogeochemical iron-cycle: A review. Biogeosciences **7**: 827–844. doi:10.5194/bg-7-827-2010

Durant, A. J., C. Bonadonna, and C. J. Horwell. 2010. Atmospheric and environmental impacts of volcanic particulates. Elements **6**: 235–240. doi:10.2113/gselements.6.4.235

Fishwick, M. P., S. J. Ussher, P. N. Sedwick, M. C. Lohan, P. J. Worsfold, K. N. Buck, and T. M. Church. 2018. Impact of surface ocean conditions and aerosol provenance on the dissolution of aerosol manganese, cobalt, nickel and lead in seawater. Mar. Chem. **198**: 28–43. doi:10.1016/j.marchem.2017.11.003

Fripiat, F., A. J. Cavagna, N. Savoye, F. Dehairs, L. André, and D. Cardinal. 2011. Isotopic constraints on the Si-biogeochemical cycle of the Antarctic Zone in the Kerguelen area (KEOPS). Mar. Chem. **123**: 11–22. doi:10.1016/j.marchem.2010.08.005

Frogner, P., S. R. Gíslason, and N. Óskarsson. 2001. Fertilizing potential of volcanic ash in ocean surface water. Geology **29**: 487–490. doi:10.1130/0091-7613(2001)029⟨0487:FPOVAI⟩2.0.CO;2

Fu, F. 2018. Etude des apports des métaux traces par le dépôt atmosphérique en Méditerranée occidentale. Univ. Paris Diderot-Paris VII.

Gassó, S., and O. Torres. 2019. Temporal characterization of dust activity in the Central Patagonia Desert (years 1964–2017). J. Geophys. Res. Atmos. **124**: 3417–3434. doi:10.1029/2018JD030209

Geisen, C. 2021. Macro- and micronutrient dissolution from desert and volcanic aerosols in rain and seawater: Impact on phytoplankton in the Southern Indian Ocean. Sorbonne Université.

Gili, S., D. M. Gaiero, S. L. Goldstein, F. Chemale, E. Koester, J. Jweda, P. Vallelonga, and M. R. Kaplan. 2016. Provenance of dust to Antarctica: A lead isotopic perspective. Geophys. Res. Lett. **43**: 2291–2298. doi:10.1002/2016GL068244

Grand, M. M., and others. 2015. Dissolved Fe and Al in the upper 1000 m of the eastern Indian Ocean: A high-resolution transect along 95°E from the Antarctic margin to the Bay of Bengal. Global Biogeochem. Cycl. **29**: 375–396. doi:10.1002/2014GB004920

Grasshoff, K., K. Kremling, and M. Ehrhardt. 1999. Methods of seawater analysis. Wiley.

Guieu, C., and others. 2010. Large clean mesocosms and simulated dust deposition: A new methodology to investigate responses of marine oligotrophic ecosystems to atmospheric inputs. Biogeosciences **7**: 2765–2784. doi:10.5194/bg-7-2765-2010

Guieu, C., F. Dulac, C. Ridame, and P. Pondaven. 2014. Introduction to project DUNE, a DUst experiment in a low nutrient, low chlorophyll ecosystem. Biogeosciences **11**: 425–442. doi:10.5194/bg-11-425-2014

Hassler, C. S., V. Schoemann, C. M. Nichols, E. C. V. Butler, and P. W. Boyd. 2011. Saccharides enhance iron bioavailability to Southern Ocean phytoplankton. Proc. Natl. Acad. Sci. **108**: 1076–1081. doi:10.1073/pnas.1010963108

Hernández-Ruiz, M., E. Barber-Lluch, A. Prieto, R. Logares, and E. Teira. 2020. Response of pico-nano-eukaryotes to inorganic and organic nutrient additions. Estuar. Coast. Shelf Sci. **235**: 106565. doi:10.1016/j.ecss.2019.106565

Hoffmann, L. J., E. Breitbarth, M. V. Ardelan, S. Duggen, N. Olgun, M. Hassellöv, and S.-Å. Wängberg. 2012. Influence of trace metal release from volcanic ash on growth of Thalassiosira pseudonana and Emiliania huxleyi. Marine Chemistry **132–133**: 28–33. doi:10.1016/j.marchem.2012.02.003.

Hoffmann, L. J., I. Peeken, and K. Lochte. 2008. Iron, silicate, and light co-limitation of three Southern Ocean diatom species. Polar Biol. **31**: 1067–1080. doi:10.1007/s00300-008-0448-6

Hutchins, D. A., P. N. Sedwick, G. R. DiTullio, P. W. Boyd, B. Quéguiner, F. B. Griffiths, and C. Crossley. 2001. Control of phytoplankton growth by iron and silicic acid availability in the Subantarctic Southern Ocean: Experimental results from the SAZ Project. J. Geophys. Res. Ocean **106**: 31559–31572. doi:10.1029/2000JC000333

Jones, M. T., and S. R. Gislason. 2008. Rapid releases of metal salts and nutrients following the deposition of volcanic ash into aqueous environments. Geochim. Cosmochim. Acta **72**: 3661–3680. doi:10.1016/j.gca.2008.05.030

Journet, E., K. V. Desboeufs, S. Caquineau, and J.-L. Colin. 2008. Mineralogy as a critical factor of dust iron solubility. Geophys. Res. Lett. **35**: L07805. doi:10.1029/2007GL031589

Krause, J. W., M. A. Brzezinski, S. B. Baines, J. L. Collier, B. S. Twining, and D. C. Ohnemus. 2017. Picoplankton contribution to biogenic silica stocks and production rates in the Sargasso Sea. Global Biogeochem. Cycl. **31**: 762–774. doi:10.1002/2017GB005619

Langmann, B., K. Zakšek, and M. Hort. 2010. Atmospheric distribution and removal of volcanic ash after the eruption of Kasatochi volcano: A regional model study. J. Geophys. Res. **115**: D00L06. doi:10.1029/2009JD013298

Li, F., P. Ginoux, and V. Ramaswamy. 2008. Distribution, transport, and deposition of mineral dust in the Southern Ocean and Antarctica: Contribution of major sources. J. Geophys. Res. **113**: D10207. doi:10.1029/2007JD009190

Lo Monaco, C., and N. Metzl. 2019. VT 163/OISO-29 cruise, RV Marion Dufresne. doi:10.17600/18000972

Mackey, K. R. M., K. N. Buck, J. R. Casey, A. Cid, M. W. Lomas, Y. Sohrin, and A. Paytan. 2012. Phytoplankton responses to atmospheric metal deposition in the coastal and open-ocean Sargasso Sea. Front. Microbiol. **3**: 1–15. doi:10.3389/fmicb.2012.00359

Mahowald, N., K. Kohfeld, M. Hansson, Y. Balkanski, S. P. Harrison, I. C. Prentice, M. Schulz, and H. Rodhe. 1999. Dust sources and deposition during the last glacial maximum and current climate: A comparison of model results with paleodata from ice cores and marine sediments. J. Geophys. Res. Atmos. **104**: 15895–15916. doi:10.1029/1999JD900084

Marañón, E., and others. 2010. Degree of oligotrophy controls the response of microbial plankton to Saharan dust. Limnol. Oceanogr. **55**: 2339–2352. doi:10.4319/lo.2010.55.6.2339

Marie, D., F. Partensky, D. Vaulot, and C. Brussaard. 1999. Enumeration of phytoplankton, bacteria, and viruses in marine samples. Curr. Protocol. Cytom. **10**: Unit 11.11. doi:10.1002/0471142956.cy1111s10

Martin, J. H. 1990. Glacial-interglacial CO_2 change: The iron hypothesis. Paleoceanography **5**: 1–13. doi:10.1029/PA005i001p00001

McClain, C. R., S. R. Signorini, and J. R. Christian. 2004. Subtropical gyre variability observed by ocean-color satellites. Deep. Res. Part II Top. Stud. Oceanogr. **51**: 281–301. doi:10.1016/j.dsr2.2003.08.002

McConnell, J. R., A. J. Aristarain, J. R. Banta, P. R. Edwards, and J. C. Simões. 2007. 20th-Century doubling in dust archived in an Antarctic Peninsula ice core parallels climate change and desertification in South America. Proc. Natl.

Acad. Sci. USA **104**: 5743–5748. doi:10.1073/pnas.0607657104

Mélançon, J., and others. 2014. Early response of the northeast subarctic Pacific plankton assemblage to volcanic ash fertilization. Limnol. Oceanogr. **59**: 55–67. doi:10.4319/lo.2014.59.1.0055

Mélançon, J., and others. 2016. Impact of ocean acidification on phytoplankton assemblage, growth, and DMS production following Fe-dust additions in the NE Pacific high-nutrient, low-chlorophyll waters. Biogeosciences **13**: 1677–1692. doi:10.5194/bg-13-1677-2016

Meskhidze, N., A. Nenes, W. L. Chameides, C. Luo, and N. M. Mahowald. 2007. Atlantic Southern Ocean productivity: Fertilization from above or below? Global Biogeochem. Cycl. **21**: 1–9. doi:10.1029/2006GB002711

Mills, M. M., C. Ridame, M. Davey, J. La Roche, and R. J. Geider. 2004. Iron and phosphorus co-limit nitrogen fixation in the eastern tropical North Atlantic. Nature **429**: 292–294. doi:10.1038/nature02550

Moore, C. M., S. Seeyave, A. E. Hickman, J. T. Allen, M. I. Lucas, H. Planquette, R. T. Pollard, and A. J. Poulton. 2007. Iron–light interactions during the CROZet natural iron bloom and EXport experiment (CROZEX) I: Phytoplankton growth and photophysiology. Deep Sea Res. Part II Top. Stud. Oceanogr. **54**: 2045–2065. doi:10.1016/j.dsr2.2007.06.011

Moore, J. K., S. C. Doney, D. M. Glover, and I. Y. Fung. 2002. Iron cycling and nutrient-limitation patterns in surface waters of the world ocean. Deep. Res. Part II Top. Stud. Oceanogr. **49**: 463–507. doi:10.1016/S0967-0645(01)00109-6

Morel, A., H. Claustre, and B. Gentili. 2010. The most oligotrophic subtropical zones of the global ocean: Similarities and differences in terms of chlorophyll and yellow substance. Biogeosciences **7**: 3139–3151. doi:10.5194/bg-7-3139-2010

Murphy, J., and J. P. Riley. 1962. A modified single solution method for the determination of phosphate in natural waters. Anal. Chim. Acta **27**: 31–36. doi:10.1016/S0003-2670(00)88444-5

Nelson, D. M., M. A. Brzezinski, D. Sigmon, and V. Franck. 2001. A seasonal progression of Si limitation in the Pacific sector of the Southern Ocean. Deep Sea Res. Part II Top. Stud. Oceanogr. **48**: 3973–3995. doi:10.1016/S0967-0645(01)00076-5

Nowak, S., S. Lafon, S. Caquineau, E. Journet, and B. Laurent. 2018. Quantitative study of the mineralogical composition of mineral dust aerosols by X-ray diffraction. Talanta **186**: 133–139. doi:10.1016/j.talanta.2018.03.059

Olgun, N., and others. 2011. Surface Ocean iron fertilization: The role of airborne volcanic ash from subduction zone and hot spot volcanoes and related iron fluxes into the Pacific Ocean. Global Biogeochem. Cycl. **25**: n/a-n/a. doi:10.1029/2009GB003761

Paris, R., K. V. Desboeufs, and E. Journet. 2011. Variability of dust iron solubility in atmospheric waters: Investigation of the role of oxalate organic complexation. Atmos. Environ. **45**: 6510–6517. doi:10.1016/j.atmosenv.2011.08.068

Paris, R., and K. V. Desboeufs. 2013. Effect of atmospheric organic complexation on iron-bearing dust solubility. Atmos. Chem. Phys. **13**: 4895–4905. doi:10.5194/acp-13-4895-2013

Paytan, A., K. R. M. Mackey, Y. Chen, I. D. Lima, S. C. Doney, N. Mahowald, R. Labiosa, and A. F. Post. 2009. Toxicity of atmospheric aerosols on marine phytoplankton, Proceedings of the National Academy of Sciences, **106**: 4601–4605. doi:10.1073/pnas.0811486106

Perron, M. M. G., M. Strzelec, M. Gault-Ringold, B. C. Proemse, P. W. Boyd, and A. R. Bowie. 2020. Assessment of leaching protocols to determine the solubility of trace metals in aerosols. Talanta **208**: 120377. doi:10.1016/j.talanta.2019.120377

Ras, J., H. Claustre, and J. Uitz. 2008. Spatial variability of phytoplankton pigment distributions in the Subtropical South Pacific Ocean: Comparison between in situ and predicted data. Biogeosciences **5**: 353–369. doi:10.5194/bg-5-353-2008

Redfield, A. C. 1934. On the proportions of organic derivatives in sea water and their relation to the composition of plankton. James Johnstone Memorial Volume. Univ. Press Liverpool, p. 176–192.

Ridame, C., J. Dekaezemacker, C. Guieu, S. Bonnet, S. L'Helguen, and F. Malien. 2014. Contrasted Saharan dust events in LNLC environments: Impact on nutrient dynamics and primary production. Biogeosciences **11**: 4783–4800. doi:10.5194/bg-11-4783-2014

Schlitzer, R. 2021. Ocean Data View, odv.awi.de.

Sedwick, P. N., S. Blain, B. Quéguiner, F. B. Griffiths, M. Fiala, E. Bucciarelli, and M. Denis. 2002. Resource limitation of phytoplankton growth in the Crozet Basin, Subantarctic Southern Ocean. Deep. Res. Part II Top. Stud. Oceanogr. **49**: 3327–3349. doi:10.1016/S0967-0645(02)00086-3

Simonella, L. E., and others. 2015. Soluble iron inputs to the Southern Ocean through recent andesitic to rhyolitic volcanic ash eruptions from the Patagonian Andes. Global Biogeochem. Cycl. **29**: 1125–1144. doi:10.1002/2015GB005177

Tagliabue, A., J. B. Sallée, A. R. Bowie, M. Lévy, S. Swart, and P. W. Boyd. 2014. Surface-water iron supplies in the Southern Ocean sustained by deep winter mixing. Nat. Geosci. **7**: 314–320. doi:10.1038/ngeo2101

Ternon, E., C. Guieu, M.-D. Loÿe-Pilot, N. Leblond, E. Bosc, B. Gasser, J.-C. Miquel, and J. Martín. 2010. The impact of Saharan dust on the particulate export in the water column of the North Western Mediterranean Sea. Biogeosciences **7**: 809–826. doi:10.5194/bg-7-809-2010

Timmermans, K. R., M. J. W. Veldhuis, P. Laan, and C. P. D. Brussaard. 2008. Probing natural iron fertilization near the

Kerguelen (Southern Ocean) using natural phytoplankton assemblages and diatom cultures. Deep Sea Res. Part II Top. Stud. Oceanogr. **55**: 693–705. doi:10.1016/j.dsr2.2007.12.008

Trimborn, S., and others. 2017. Iron sources alter the response of Southern Ocean phytoplankton to ocean acidification. Mar. Ecol. Prog. Ser. **578**: 35–50. doi:10.3354/meps12250

Twining, B. S., S. Rauschenberg, S. E. Baer, M. W. Lomas, A. C. Martiny, and O. Antipova. 2019. A nutrient limitation mosaic in the eastern tropical Indian Ocean. Deep. Res. Part II Top. Stud. Oceanogr. **166**: 125–140. doi:10.1016/j.dsr2.2019.05.001

Uitz, J., H. Claustre, A. Morel, and S. B. Hooker. 2006. Vertical distribution of phytoplankton communities in open ocean: An assessment based on surface chlorophyll. J. Geophys. Res. **111**: C08005. doi:10.1029/2005JC003207

Wagener, T., E. Pulido-Villena, and C. Guieu. 2008. Dust iron dissolution in seawater: Results from a one-year time-series in the Mediterranean Sea. Geophys. Res. Lett. **35**: 1–6. doi:10.1029/2008GL034581

Watson, A. J., D. C. E. Bakker, A. J. Ridgwell, P. W. Boyd, and C. S. Law. 2000. Effect of iron supply on Southern Ocean CO_2 uptake and implications for glacial atmospheric CO_2. Nature **407**: 730–733. doi:10.1038/35037561

Wei, Y., J. Sun, Z. Chen, Z. Zhang, G. Zhang, and X. Liu. 2021. Significant contribution of picoplankton size fraction to biogenic silica standing stocks in the Western Pacific Ocean. Prog. Oceanogr. **192**: 102516. doi:10.1016/j.pocean.2021.102516

Witham, C. S., C. Oppenheimer, and C. J. Horwell. 2005. Volcanic ash-leachates: A review and recommendations for sampling methods. J. Volcanol. Geotherm. Res. **141**: 299–326. doi:10.1016/j.jvolgeores.2004.11.010

Wuttig, K., and others. 2019. Critical evaluation of a seaFAST system for the analysis of trace metals in marine samples. Talanta **197**: 653–668. doi:10.1016/j.talanta.2019.01.047

Acknowledgments

The study has been financed by the French Research Program LEFE (Les Enveloppes Fluides et l'Environnement) through BISOU and ITALIANO projects and by the DADDY project supported by IPSL. The authors thank INSU and the French oceanographic fleet ("Flotte océanographique française") for financial and logistic support to the OISO program and the VT163/OISO-29 oceanographic campaign (https://doi.org/10.17600/18000972). The authors thank the PACHIDERM analytical platform (LEMAR) for NOx and trace metal analysis; I. Djouraev (LOCEAN) for ICP-MS analysis at the Alysés platform, IRD; M. Benrahmoune and F. Kaczmar (LOCEAN) for managing clean labs and help in sample processing; F. Fu (LISA) for acid attack of aerosols; M. Mandeng-Yogo (LOCEAN) for IR-MS and CN analysis at the Alysés platform, IRD; S. Nowak (LISA) for XRS analysis at Paris Diderot University; I. Obernosterer and P. Catala (LOMIC) for inter-comparison of flow cytometric data; L. Sicard (ITODYS) and M. Jean Pierre (LISA) for nitrogen BET analysis and C. Vaulot (IS2M) for SSA and krypton BET analysis. D. Lannuzel, B. Moriceau and two anonymous reviewers are thanked for providing relevant comments on the manuscript.

Conflict of Interest

None declared.

Submitted 30 June 2021
Revised 18 December 2021
Accepted 28 April 2022

Associate editor: Laura Bristow